

Effect of Streamwise Spacing on the Sound Generated by Flow through Two Square Cylinders in Tandem Arrangement



B. Manshoor^{1*}, I. Zaman², A. Khalid³, M.F. Ghazali⁴, Manish K. Khandelwal⁵,

¹Flow Analysis, Simulation, and Turbulence Research Group (FASTREG),
Faculty of Mechanical and Manufacturing Engineering,
Universiti Tun Hussein Onn Malaysia, MALAYSIA

²Noise, Vibration and Acoustic Research Group (NOVA),
Faculty of Mechanical and Manufacturing Engineering,
Universiti Tun Hussein Onn Malaysia, MALAYSIA

³Advanced Technology Centre (ATC), Faculty of Engineering Technology,
Universiti Tun Hussein Onn Malaysia, MALAYSIA

⁴Advanced Structural Integrity and Vibration Research (ASIVR),
Faculty of Mechanical Engineering, Universiti Malaysia Pahang, MALAYSIA

⁵Dept. of Mathematics, Indira Gandhi National Tribal University, INDIA

*:bukhari@uthm.edu.my

ABSTRACT

The sound generated by the flow past two square cylinder in tandem arrangements was investigated by direct solution of two dimensional, unsteady, compressible Navier-Stokes equation. The main objective of the investigation is to study the effect of the spacing between two square cylinders on the generation and propagation mechanism of the sound. Since the sound pressure is very small compared to normal pressure and other parameters, high order computational scheme was used to capture the pressure fluctuations. Besides that, filtering is employed to eliminate the high frequency part caused by nonlinearity of the governing equations. 4th order Runge-Kutta method was employed for time marching and for the boundary condition, adiabatic and non-slip conditions are imposed on the surface of the square cylinders. Present results for near-field flow features are in good agreement with the experimental results by previous researchers though the Reynolds number ranges examined are different. From the results, it shows that tandem arrangement of two cylinders with a small spacing may be useful for a passive control to reduce the generated sound since the larger spacing ($L/D > 4$), the shear layer separated from the upstream cylinder rolls up and forms vortices in front of the downstream cylinder. The results also showed that body-vortex interaction enhances the amplitude of the generated sound significantly.

Key words : Body-Vortex Interaction, Sound propagation, Tandem cylinders.

1. INTRODUCTION

Many numerical and experimental studies have been carried out to understand the characteristics of the flow around a bluff body. Rectangular cylinder is one of the typical examples of the bluff body, and a number of studies on the flow around rectangular cylinders have

been done both experimentally (Okajimaj [1], Knisely [2], Norberg [3], Lyu *et al.* [4]) and computationally (Davis and Moore [5], Franke *et al.* [6], Manshoor [7], Kelkar and Patankar [8]).

Flow past two square cylinders in a tandem arrangement is one of the simplified cases of the flow past an array of cylinders, and has important engineering applications, including heat exchangers, electronic devices and so on [9]. It is well known that the flow pattern around two cylinders in a tandem arrangement depends strongly on the spacing between the centers of the cylinders. Sakamoto *et al.* [10] experimentally investigated forces acting on two square cylinders in a tandem arrangement in a uniform flow. The Reynolds numbers examined were 2.76×10^4 and 5.52×10^4 . They observed due to different flow patterns below and above a critical spacing between the centers of the cylinders. The critical value was $L/D = 4$ where L is the spacing between the centers of the two cylinders and D is the cylinder diameter. $L/D = 4$, two different values of the mean drag coefficient C_d and the Strouhal number, S_r were observed due to the existence of the two flow patterns. Similar results were also obtained in the experiment of Luo and Teng [11] where the Reynolds number was 5.67×10^4 . Liu and Chen [12] experimentally studied the flow characteristics around two square cylinders in a tandem arrangement. The spacing L/D ranged from 1.5 to 9 and the Reynolds number ranged from 2.0×10^3 and 1.6×10^4 . They showed that hysteresis with two discontinuous jumps was present for all Reynolds numbers studied when the spacing was varied in two different ways, one being progressive increase and other a progressive decrease.

The hysteresis was associated with the existence of two different flow patterns. In one flow pattern which appeared when the spacing was small, the roll-up of the shear layer separated from the upstream cylinder is suppressed called *Mode I*. In the other flow pattern which appeared with increased spacing beyond a critical value, the shear layer separated from the

upstream cylinder rolled to periodically form vortices and the rolled-up vortices interact with the downstream cylinder, named *Mode II*. The discontinuous jump were attributed to a sudden change of the flow pattern between the two types of flow. Liu and Chen [12] also observed two C_d values at each L/D in the hysteresis regime for both upstream and downstream cylinders which were associated with the existence of the two different flow patterns. Two values at each L/D in the hysteresis regime were also observed for S_r .

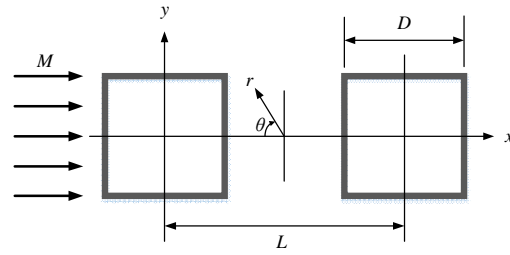


Figure 1: Schematic diagram of the flow.

Research of the sound generated by the flow around a bluff body (so called aeolian tone) has a long history of more than hundred years. A brief reviews on the aeolian tone for the case of a circular cylinder has been given by Inoue and Hatakeyama [13], and that for the case of a square cylinder have been given by Imamura *et al.* [14]. In engineering applications, the sound generated by two or more square cylinders in a tandem arrangement is important; typical examples are electronic devices, heat exchangers and low-rise building roofs.

The objective in this research is to study the generation and propagation mechanism of the sound generated by the flow past two square cylinders in a tandem arrangement. This study also aims to increase our understanding of the basic nature of the sound generated from bluff bodies. Special attention is paid to the effect of the spacing between the two cylinders on the generation mechanism of the sound. The sound generation by a single square cylinder is included in this study as a special case where the spacing vanishes.

2. FLOW MODEL AND PARAMETERS

A schematic diagram of the flow model is presented in Figure 1. An upstream cylinder is fixed at the origin. The coordinates parallel and normal to the free stream are denoted by x and y , respectively. The origin of the polar coordinates (r, θ) which is used for discussion of far-field acoustic quantities, is placed at the midpoint of the two cylinders. The symbol L denotes the spacing between the centers of the two cylinders. The lengths are made dimensionless by the cylinder diameter D and the velocity is scaled by the speed of sound, c . The time and density are made dimensionless by D/c and the ambient density, ρ respectively. The normalized spacing L/D is prescribed to be in the range of $0 \leq L/D \leq 7$. The Mach number of a uniform flow is defined by $M_a = U/c$ where U denotes the velocity of the uniform flow. The Reynolds number is defined as $Re = UD/\nu$ where ν is the kinematic viscosity. In this study, the Reynolds number is fixed to be 150, and the Mach number is 0.2.

3. NUMERICAL PROCEDURE

3.1. Governing equations

Governing equations are the two-dimensional, unsteady, compressible, Navier-Stokes equations. Ideal gas is adopted. The continuity equation is,

$$\frac{\partial}{\partial t}(\rho) + \frac{\partial}{\partial x}(\rho u) + \frac{\partial}{\partial y}(\rho v) = 0 \quad (1)$$

The momentum equation are,

$$\begin{aligned} \frac{\partial}{\partial t}(\rho u) + \frac{\partial}{\partial x}(\rho u^2 + p) + \frac{\partial}{\partial y}(\rho uv) \\ = \frac{\partial}{\partial x}(\tau_{xx}) + \frac{\partial}{\partial y}(\tau_{xy}) \end{aligned} \quad (2)$$

$$\begin{aligned} \frac{\partial}{\partial t}(\rho v) + \frac{\partial}{\partial y}(\rho v^2 + p) + \frac{\partial}{\partial x}(\rho uv) \\ = \frac{\partial}{\partial x}(\tau_{yx}) + \frac{\partial}{\partial y}(\tau_{yy}) \end{aligned} \quad (3)$$

The energy equation is,

$$\begin{aligned} \frac{\partial e}{\partial t} + \frac{\partial}{\partial x}[(e + p)u] + \frac{\partial}{\partial y}[(e + p)v] = \\ \frac{\partial}{\partial x}\left(u\tau_{xx} + v\tau_{xy} + \kappa\frac{\partial T}{\partial x}\right) + \\ \frac{\partial}{\partial y}\left(u\tau_{yx} + v\tau_{yy} + \kappa\frac{\partial T}{\partial y}\right) \end{aligned} \quad (4)$$

4. COMPUTATIONAL SCHEME

a. Spatial derivatives

The 8th-order Padé type compact scheme is applied for the spatial derivatives [15]. The reason why such a high order scheme is applied in this study is that the sound pressure is very small compared to normal pressure and other parameters. To capture the small value of the pressure fluctuation, a high-order scheme is necessary. For simplicity, consider a uniformly spaced mesh where the nodes are indexed by i . The independent variable values at the nodes is $x_i = h(i-1)$ for $1 \leq i \leq N$ and the function values at the nodes $f_i = f(x_i)$ are given. The finite difference approximation f'_i to the first derivative $(df/dx)(x_i)$ at the node i depends on the function values at nodes near i . The procedure of the scheme is shown here. When the grid width is fixed at h , pentadiagonal scheme is expressed as,

$$\begin{aligned} \xi f'_{i-2} + \eta f'_{i-1} + f'_i + f'_{i+1} + f'_{i+2} \\ = a \frac{f'_{i+1} - f'_{i-1}}{2h} + b \frac{f'_{i+2} - f'_{i-2}}{4h} \\ + c \frac{f'_{i+3} - f'_{i-3}}{6h} \end{aligned} \quad (5)$$

The procedure for the second derivatives is same as that for the first derivatives. The pentadiagonal Padé compact scheme for the second derivative f''_i is expressed as,

$$\begin{aligned} & \xi f''_{i-2} + \eta f''_{i-1} + f''_i + f''_{i+1} + f''_{i+2} \\ & = a \frac{f'_{i+1} - f'_{i-1}}{h^2} + b \frac{f'_{i+2} - f'_{i-2}}{(2h)^2} \\ & + c \frac{f'_{i+3} - f'_{i-3}}{(3h)^2} \end{aligned} \quad (6)$$

b. Filtering and Time Marching

Filtering is employed to eliminate the high-frequency part caused by nonlinearity of the governing equation, i.e. Navier-Stokes. The 4th-order tridiagonal Padé filter is used for filtering. The filtered function \hat{f}_i is written as,

$$\begin{aligned} & \xi \hat{f}_{i-2} + \eta \hat{f}_{i-1} + \hat{f}_i + \hat{f}_{i+1} + \hat{f}_{i+2} \\ & = \alpha_3 \hat{f}_i + \frac{c_3}{2} (f_{i+2} - f_{i-2}) \\ & + \frac{b_3}{2} (f_{i+1} - f_{i-1}) \end{aligned} \quad (7)$$

Since the calculation for the time-marching in this research also requires a high accuracy, the 4th-order Runge-Kutta method is employed for the calculation.

c. Boundary condition

Adiabatic and non-slip conditions are imposed on the surface of the body.

$$\frac{\partial T}{\partial n} = 0 \quad \text{and} \quad u = v = 0 \quad (8)$$

where \mathbf{n} is a unit normal vector perpendicular to the surface of a cylinder. Navier-Stokes Characteristic Boundary Conditions is applied for the near field, which is a non-reflecting condition and removes numerical reflection. Only waves moving from the boundary to the outside are concerned and waves from outside to the region of the calculation are excluded. The two-dimensional Navier-Stokes equations (1)-(4) are modified.

$$\frac{\partial}{\partial t}(\rho) + d_1 + \frac{\partial}{\partial y}(\rho v) = 0 \quad (9)$$

$$\begin{aligned} & \frac{\partial}{\partial t}(\rho u) + u d_1 + \rho d_3 + \frac{\partial}{\partial y}(\rho u v) \\ & = \frac{\partial}{\partial x}(\tau_{xx}) + \frac{\partial}{\partial y}(\tau_{yx}) \end{aligned} \quad (10)$$

$$\begin{aligned} & \frac{\partial}{\partial t}(\rho v) + v d_1 + \rho d_4 + \frac{\partial}{\partial y}(\rho u^2 + p) \\ & = \frac{\partial}{\partial x}(\tau_{xy}) + \frac{\partial}{\partial y}(\tau_{yy}) \end{aligned} \quad (11)$$

$$\begin{aligned} & \frac{\partial e}{\partial t} + \frac{d_2}{\gamma-1} + \rho u d_3 + \rho v d_4 + \frac{\partial}{\partial y}[(e+p)v] \\ & = \frac{\partial}{\partial x}\left(u\tau_{xx} + u\tau_{xy} + \kappa \frac{\partial T}{\partial t}\right) \\ & + \frac{\partial}{\partial y}\left(u\tau_{xy} + v\tau_{yy} + \kappa \frac{\partial T}{\partial t}\right) \end{aligned} \quad (12)$$

5. GENERATION OF GRID SYSTEM

The grid is a non-uniform rectangular grid. The computational domain is divided into three regions of different grid spacings, as in Figure 2.

- Flow region $[0 \leq x \leq x_{min}], [0 < y < y_{min}]$
- Vortex region $[x_{min} \leq x \leq x_{mid}], [y_{min} < y < y_{mid}]$
- Buffer region $[x_{mid} \leq x \leq x_{buffer}], [y_{mid} < y < y_{buffer}]$

The spacing in the surface region is prescribed to be fine enough to analyze the boundary layer on the cylinder surfaces. The vortex region is set outside the flow region to capture sound waves propagating to the far field. In addition, the buffer region is set for the suppression of the wave reflection. The areas between the different grid widths regions are connected by a hyperbolic tangent function to let the grid width become wider smoothly, as shown in Figure 3. The growth rate of the grid width between the flow region and vortex region is within 4%, and that of the grid between the vortex region and the buffer region is within 9%.

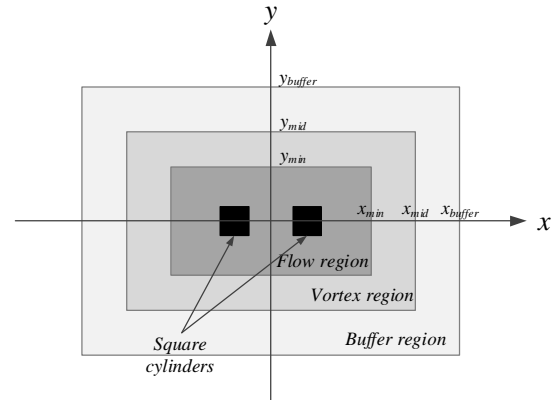


Figure 2: Computational domain.

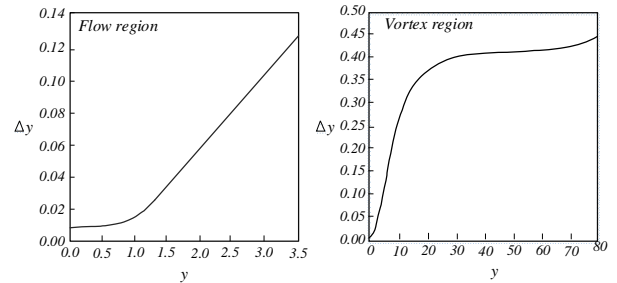


Figure 3: Distribution of grid spacing in flow and vortex region.

6. RESULTS AND DISCUSSION

a. Force acting on the cylinders

Figure 4 shows typical examples of time-histories of the drag and lift force acting on the two cylinders for the single case which is $L/D = 0$ and *Mode I* which is $L/D = 3$. The essential features of the forces acting on the upstream and downstream square cylinders are the same as those for a single square cylinder. The amplitude of the lift coefficient, C_l is larger than that of the drag coefficient, C_d and the frequency of C_d is twice as high as that of C_l . It should be noted that the amplitudes of the fluctuations of both C_d and C_l are

larger on the downstream cylinder than on the upstream cylinder in the cases of the two cylinders. In the case of *Mode I*, the amplitudes of the lift and drag of both the upstream and downstream cylinders are much smaller than those of single cylinder case, because no vortex shedding occurs from the upstream cylinder and no interaction of shed vortices with the downstream cylinder occurs.

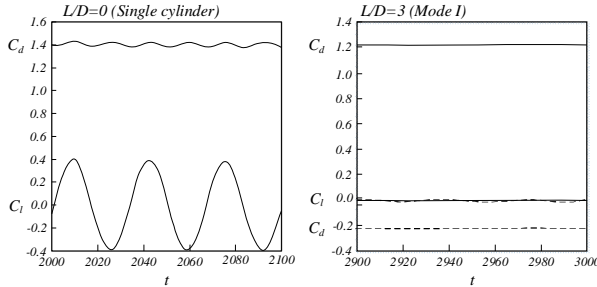


Figure 4: Time histories of the lift C_l and drag C_d coefficient for single cylinder and *Mode I* flow. (— upstream, ---- downstream)

As shown in Figure 5 for the case of *Mode II*, which are $L/D = 3.5$ and 5 , amplitudes of the lift and drag of both the upstream and downstream cylinders are much larger than those of the single cylinder case. It is well known that the fluctuations of the forces are deeply related to the sound generation [13], [16]. The results shown in Figure 5 suggest that the sound generated by the two cylinders may be much smaller than that generated by the single cylinder in *Mode I* and that the sound generated by the two cylinders in *Mode II* may be much larger than that generated by the singled cylinder. The results shown in Figure 5 for both cases suggest that the sound generated by the downstream cylinder may be larger than that generated by the upstream cylinder.

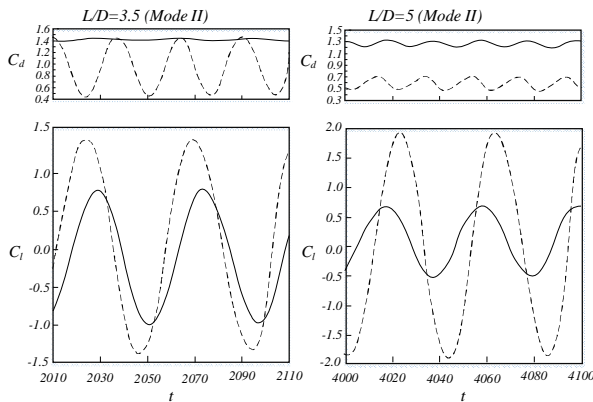


Figure 5: Time histories of the lift C_l and drag C_d coefficient for $L/D = 3.5$ and 5 . (— upstream, ---- downstream)

The mean drag coefficient, C_d and the Strouhal number, S_f for the case of $M_a = 0.2$ and $Re = 150$ are presented in Figure 6 against the spacing L/D . For the mean drag coefficient, it shows that C_d has two values at $L/D = 3.5$ and 4 for both the upstream and downstream cylinders which corresponds to the appearance of either of the

two flow patterns, *Mode I* and *Mode II*, depending on the initial conditions. It may be also interesting to see in the figure that C_d of the downstream cylinder shows negative values for *Mode I*, in agreement with the experimental observations of Sakamoto *et al.* [9], Luo and Teng [11] and Liu and Chen [12]. The Strouhal number, S_f was obtained from the fluctuation of the lift coefficient C_l which is the same for the upstream and downstream cylinders, as we can see from Figures 5, in agreement with the experimental observation of Sakamoto *et al.* [10]. In Figure 6 for the Strouhal number, it shows that the S_f also has two values at $L/D = 3.5$ and 4 , respectively. The present computational results shown in Figure 6 are in agreement with the experimental observations of Liu and Chen [12], Sakamoto *et al.* [10] and Luo and Teng [11], though $Re = 150$ this study is much smaller than those in the experiments.

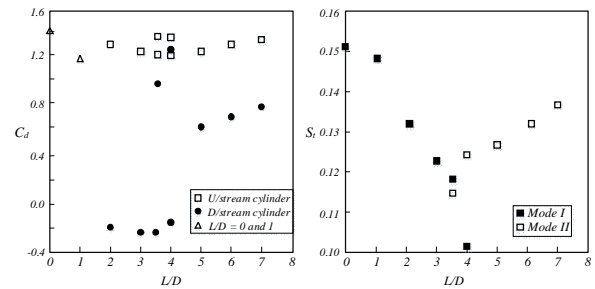


Figure 6: Effect of the spacing L/D on the drag coefficient, C_d and Strouhal number, S_f .

As already noted before, the generation of aeolian tone is related to the fluctuations of forces acting on a cylinder. Presented in Figure 7 is the variation with L/D of the amplitudes of the fluctuations of the lift and drag coefficients, $C_{l,amp}$ and $C_{d,amp}$, for the case of $M_a = 0.2$ and $Re = 150$. Figure 7 shows that both $C_{l,amp}$ and $C_{d,amp}$ in *Mode I* on both the upstream and downstream cylinders are much smaller than those on the single cylinder, and that those in *Mode II* are much larger than those on the single cylinder. Figure 7 also shows that both $C_{l,amp}$ and $C_{d,amp}$ in *Mode II* are much larger on the downstream cylinder than on the upstream cylinder, irrespective of the spacing $L/D \geq 3.5$, and that both $C_{l,amp}$ and $C_{d,amp}$ have two values at $L/D = 3.5$ and 4 , respectively. These results suggest that the generation mechanism of the aeolian tone may be different for the two modes and that the magnitude of the aeolian tone may be larger in *Mode II* than in *Mode I*. In the following, we try to clarify the difference of the generation mechanism of the sound between the two modes.

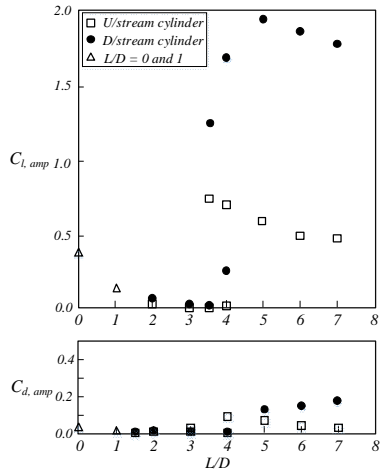


Figure 7: Effect of the spacing L/D on fluctuations of the lift and drag coefficient.

b. Pressure fluctuations around the upstream cylinders

The fluctuation pressure Δp on the cylinder surfaces for the case of *Mode II* is defined by $\Delta p = p - p_\infty$, which is the time-averaged pressure. The symbol p_∞ denotes the ambient pressure. The fluctuation pressure Δp was measured at each three locations on the upstream and downstream cylinders; (1) the midpoints on the upper surfaces, A and A' , (2) the midpoints on the lower surfaces, B and B' , and (3) the midpoints on the upstream surfaces C and C' , as in Figure 8.

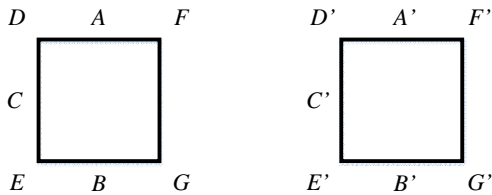


Figure 8: Typical observation points on the cylinders surface.

Time histories of the fluctuation pressure Δp on the upstream cylinder surfaces for the case of *Mode II* with $L/D = 3.5$ and $L/D = 5$ are presented in Figure 9. From the figure, we can see that the pressure fluctuations on the upper and lower surfaces are 180° phase difference, showing a dipolar nature of Δp . The amplitudes of Δp on the upper and lower surfaces, A and B are larger than those on the upstream surfaces, C , indicating that the lift dipole dominates the pressure fluctuation. These results are in agreement with the fluctuations of C_d and C_l shown in Figure 5.

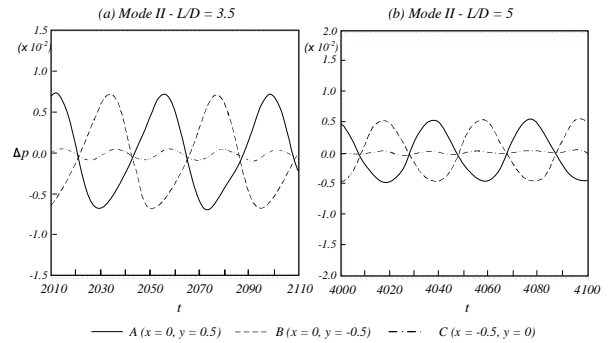


Figure 9: Time histories of the pressure fluctuations, Δp at the surface of the upstream cylinders for *Mode II*. ($L/D = 3.5$ and 5)

Now, let us consider the relation between the lift forces acting on the cylinders and pressure fluctuations near the cylinders. In Figure 5, C_l on the upstream cylinder takes one of its positive peaks at $t \approx 2030$, showing that an upward lift force is acting on the cylinder. In other words, around this instant, Δp is negative on the upper side of the cylinder whereas it is positive on the lower side. In fact, Figure 9 for $L/D = 3.5$, it shows that around this instant measured at the location A on the upper side is negative and that measured at B on the lower side is positive. The figure also shows that the profiles of Δp measured on the upper and lower surfaces on the upstream cylinders are deformed from the sinusoidal form which is observed for a single cylinder/square cylinder [13].

For the two cylinders case, body-vortex interaction may affect the pressure fluctuation around the upstream cylinder. The deformed profiles of Δp in Figure 9 are attributed to the effect of body-vortex interaction. As an evidence, time histories of Δp on the cylinder surfaces for a larger spacing of $L/D = 5$ are presented in the Figure 9 for comparison. By comparing the both results, we can see that the profiles of Δp on the upstream cylinder are more sinusoidal for $L/D = 5$ than those for $L/D = 3.5$. This is because the effect of body-vortex interaction on Δp on the upstream cylinder decreases with increasing L/D . From both results also we may say that the pressure fluctuation around the upstream cylinder in *Mode II* is generated mainly by the vortex shedding from the upstream cylinder, and that the effect of body-vortex interaction on it is minor. As shown Figure 7, the amplitude of the lift of the upstream cylinder decreases with increasing spacing L/D between the two cylinders, because the effect of body-vortex interaction decreases with increasing L/D .

Body-vortex interaction affects also the surface pressure fluctuations on the upstream cylinder, as shown in Figure 10 for $L/D = 3.5$ and 5 . The effect of body-vortex interaction first appears in a flow near the downstream surface of the upstream cylinder. Taking these points into consideration, Δp was measured at the following eight locations; (1) at the upstream two corners of the upstream cylinder, D and E ; (2) at the downstream two corners of the upstream cylinder, F and G ; as in Figure 8.

From the figure, it shows that the profiles of Δp measured at the downstream corners (F and G) of the upstream cylinder are more deformed, due to the effect of body-vortex interaction than those at both the upstream corners (D and E). Again the profiles measured at the downstream corners of the upstream cylinder for $L/D = 5$, shown in Figure 10 are more sinusoidal than those for $L/D = 3.5$, due to the smaller effect of body-vortex interaction on the upstream cylinder for $L/D = 5$.

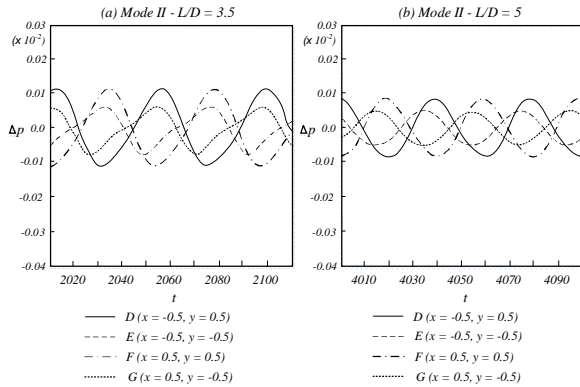


Figure 10: Time histories of the pressure fluctuations, Δp at the corner of the upstream cylinders for *Mode II*. ($L/D = 3.5$ and 5)

c. Pressure fluctuations around the downstream cylinders

On the downstream cylinder, C_1 in Figure 5 ($L/D = 3.5$) takes one of its positive peaks at $t \approx 2025$ (and ≈ 2070) and a negative peak at $t \approx 2045$ (and ≈ 2095). In agreement with the negative peak in Figure 5 ($L/D = 3.5$), Figure 11 shows that Δp measured at the location A' on the upper side is positive and that measured at B' on the lower side is negative at $t \approx 2045$, which is vice versa for the positive peak of C_1 at $t \approx 2025$ (and ≈ 2070).

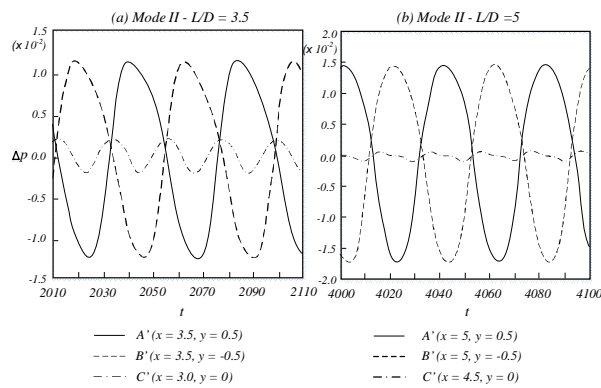


Figure 11: Time histories of the pressure fluctuations, Δp at the surface of the downstream cylinders for *Mode II*. ($Re = 150, L/D = 3.5$)

Again, it can see that the effect of body-vortex interaction first appears in a flow near the downstream surface of the upstream cylinder. The points that was

taking for consideration to measure Δp are at the following eight locations; (1) at the upstream two corners of the upstream cylinder, D' and E' ; (2) at the downstream two corners of the upstream cylinder, F' and G' ; as in Figure 8. In the Figure 11, it shows that the profiles of Δp measured at the downstream corners (F' and G') of the downstream cylinder are double-peaked whereas those measured at the upstream corners (D' and E') are single-peaked. The double-peaked profiles at F' and G' show that the pressure fluctuations near the downstream corners are generated by both body-vortex interaction and the vortex shedding.

On the other hand, the single peaked profiles at D' and E' show that the pressure fluctuations near the upstream corners are generated mainly by body-vortex interaction and that the effect of the vortex shedding is not large enough to deform the profiles at the upstream corners. Similar double-peaked profiles at the downstream corners and single-peaked profiles at the upstream corners of the downstream cylinder are also observed for $L/D = 5$, as shown in Figure 12. Both cases of *Mode I* and *Mode II* in the figure also show that the magnitudes of Δp at the upstream corners are larger than those at the downstream corners. These results show that body-vortex interaction has a larger effect than the vortex shedding on the generation of the pressure fluctuation around the downstream cylinder.

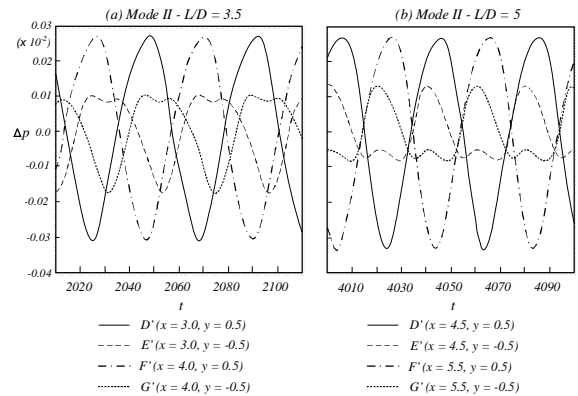


Figure 12: Time histories of the pressure fluctuations, Δp at the corner of the cylinders for *Mode II*. ($Re = 150, L/D = 5$)

As already noticed before in Figure 5 for $L/D = 3.5$, C_1 on the downstream cylinder takes one of its positive peaks at $t \approx 2025$ (and ≈ 2070) and a negative peak at $t \approx 2045$ (and ≈ 2095). Figure 12 shows that Δp measured at G' takes its negative peak at $t \approx 2030$ whereas Δp at E' takes its negative peak at $t \approx 2050$ which is much closer to the time of the negative peak of C_1 at $t \approx 2045$. The negative peak of Δp at G' is generated by the vortex shedding from the lower side of the downstream cylinder whereas that at E' is generated by body-vortex interaction. Therefore, the result shown in Figure 12 indicates that the effect of body-vortex interaction on the negative peak of C_1 is larger than the effect of the vortex shedding. Similarly, it can be seen that the positive peak of C_1 at $t \approx 2025$ (and ≈ 2070) is also affected mainly by body-vortex interaction.

The lift coefficient C_l is obtained by integrating Δp over the upper and lower cylinder surfaces. Figure 13 shows R.M.S distributions of Δp on the upper and lower surfaces of both the upstream and downstream cylinder's surfaces. From Figure 13, it shows that the magnitude of Δp fluctuation on the downstream cylinder is much larger than that on the upstream cylinder on the upstream part of the cylinder D (E) and D' (E') in Figure 8, and that Δp on the downstream cylinder decrease monotonically with increasing distance x from D' (E') to F' (G'). This results show that the lift force fluctuation on the downstream cylinder is generated more on the upstream part than on the downstream part, indicating that the lift force fluctuation is produced mainly by body-vortex interaction. Similar results are also obtained in the other cases of L/D in *Mode II*.

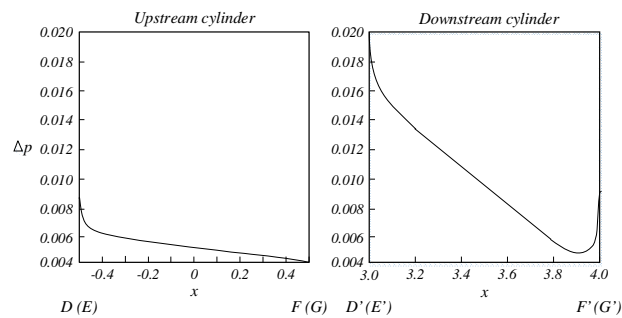


Figure 13: The distributions of R.M.S of the pressure fluctuations on the cylinders ($Re = 150$, $L/D = 3.5$)

All the results shown in this section show that body-vortex interaction plays a primary role in the generation of the pressure fluctuation around the downstream cylinder.

7. CONCLUSION

The sound generated by two square cylinders placed in a tandem arrangement in a uniform flow at low Mach number has been studied by direct numerical simulation of the two-dimensional unsteady compressible Navier-Stokes equations. The effect of the spacing L/D between the centers of the two cylinders on the generation mechanism of the sound has been investigated in detail. Present computational results for near-field flow features are in good agreement with the experimental observations by previous researcher [10-12] though the Reynolds number ranges examined are different.

This result suggests that tandem arrangement of two cylinders with a small spacing may be useful for a passive control to reduce the generated sound. When the spacing is large ($L/D > 4$), the shear layer separated from the upstream cylinder rolls up and forms vortices in front of the downstream cylinder (*Mode II*). The rolled up vortices interact with the downstream cylinder (body-vortex interaction) and generate the pressure fluctuation around the downstream cylinder. Therefore, in *Mode II*, pressure fluctuations are generated mainly by body-vortex interaction. The effect

of body-vortex interaction on the pressure fluctuation around the upstream cylinder is minor. On the other hand, body-vortex interaction plays a primary role in the generation of the pressure fluctuation from the downstream cylinder. The present result has shown that the pressure wave generated near the downstream cylinder by body-vortex interaction is dominant and body-vortex interaction has a primary effect on the sound generation in *Mode II*. The magnitude of the generated sound is much larger in *Mode II* than both *Mode I* and the single cylinder case. The magnitude at $L/D = 3.5$ in *Mode II* was more than 300 times as large as that at $L/D = 3.5$ in *Mode I* and more than four times as large as that in the single square cylinder case. These results show that body-vortex interaction enhances the amplitude of the generated sound significantly. In the range of L/D between 3.5 and 4, either *Mode I* or *Mode II* appears depending on the initial condition. Both the mean drag coefficient C_d and the Strouhal number S_t have two values at $L/D = 3.5$ and 4, respectively.

ACKNOWLEDGEMENT

The authors thank the Ministry of Higher Education, MALAYSIA (MOHE) and Universiti Tun Hussein Onn Malaysia (UTHM) for the award of post doctorate sponsorship under the staff development programme. Special thanks to Institute of Fluid Science, Tohoku University, Japan for providing facilities for this research.

REFERENCES

- [1] Okijama, A. "Strouhal numbers of rectangular cylinders", *Journal of Fluid Mechanics*, Vol. 123 (1982), pp.379-398.
<https://doi.org/10.1017/S0022112082003115>
- [2] Knisely, C.E. "Strouhal numbers of rectangular cylinders at incidence: A review and new data", *Journal of Fluids and Structures*, Vol. 4, No. 4, (1990), pp.371-393.
- [3] Norberg, C.E. "Flow around rectangular cylinders: Pressure forces and wake frequencies", *Journal of Wind Engineering and Industrial Aerodynamics*, Vol. 49, No. 1-3, (1993), pp.187-196.
- [4] Lyu, D.A., Rodi, W. and Park, J.H.C.E. "A laser-doppler velocimetry study of ensemble-averaged characteristics of the turbulent near wake of a square cylinder", *Journal of Fluid Mechanics*, Vol. 304 (1995), pp.285-319.
- [5] Davis, R.W. and Moore, E.F. "A numerical study of vortex shedding from rectangles", *Journal of Fluid Mechanics*, Vol. 116 (1982), pp.475-506.
- [6] Franke, R., Rodi, W. and Schonung, B. "Numerical calculation of laminar vortex flow past cylinders", *Journal of Wind Engineering and Industrial Aerodynamics*, Vol. 35, (1990), pp.237-257.
- [7] Manshoor, B. and Khalid, A. "Numerical investigation of the circle grids fractal flow conditioner for orifice plate flowmeters", *Applied Mechanics and Materials*. Vol. 229, No. 231 (2012), pp.700-704.
[doi:10.4028/www.scientific.net/AMM.229-231.700](https://doi.org/10.4028/www.scientific.net/AMM.229-231.700)

- [8] Kelkar, K.M. and Patankar, S.V. "Numerical prediction of vortex shedding behind a square cylinder", *International Journal for Numerical Methods in Fluids*, Vol. 14, No. 3 (1992), pp.327-341.
<https://doi.org/10.1002/flid.1650140306>
- [9] Manshoor, B., Jaat, M., Izzuddin, Z., and Khalid, A. "CFD analysis of thin film lubricated journal bearing", *Procedia Engineering*, Vol. 68 (2013) pp.56-62. doi:10.1016/j.proeng.2013.12.147
- [10] Sakamoto, H., Haniu, H. and Obata, Y. "Fluctuating forces acting on two square prisms in a tandem arrangement", *Journal of Wind Engineering and Industrial Aerodynamics*, Vol. 26, No.1 (1987), pp.85-103
- [11] Luo, S.C. and Teng, T.C. "Aerodynamic forces on a square section cylinder that is downstream to an identical cylinder", *The Aeronautical Journal*, Vol. 94, No. 936 (1990) pp.203-212.
- [12] Liu, C.H. and Chen, J.M. "Observations of hysteresis in flow around two square cylinders in a tandem arrangement", *Journal of Wind Engineering and Industrial Aerodynamics*, Vol. 90, No. 9, (2002), pp.1019-1050.
- [13] Inoue, O. and Hatakeyama, N. "Sound generation by a two-dimensional circular cylinder in a uniform flow," *Journal of Fluid Mechanics*, Vol. 471 (2002), pp.285-314.
<https://doi.org/10.1017/S0022112002002124>
- [14] Imamura, A., Hatakeyama, N. & Inoue, O. "Numerical analysis of sound generation by a two-dimensional cylinder in a uniform flow," *Proceedings of the 4th ASME/JSME Joint Fluid Engineering Conference*, FEDSM2003-45754, (2003).
- [15] Lele, S.K. "Compact finite difference schemes with spectral-like resolution", *Journal of Computational Physics*, Vol. 103, No. 1 (1992), pp.16-42.
- [16] Curle, N. "The influence of solid boundaries upon aerodynamics", *Proc. Of the Royal Society A*, Vol. 231, No. 1187 (1955), 505.
DOI: 10.1098/rspa.1955.0191